arXiv:1610.02556v1 [cond-mat.quant-gas] 8 Oct 2016

# Local Quench, Majorana Zero Modes, and Disturbance Propagation in the Ising chain

G. Francica,[1,2] T. J. G. Apollaro,[3] N. Lo Gullo,[4] and F. Plastina[1,2]

[1]*Dipartimento di Fisica, Universitá della Calabria, 87036 Arcavacata di Rende (CS), Italy*
[2]*INFN - Gruppo Collegato di Cosenza*
[3]*NEST, Istituto Nanoscienze-CNR and Dipartimento di Fisica e Chimica, Università degli Studi di Palermo, via Archirafi 36, I-90123 Palermo, Italy*
[4]*Dipartimento di Fisica, Università degli Studi di Milano, via Celoria 16, 20133, Milano, Italy*

(Dated: October 11, 2016)

We study the generation and propagation of local perturbations in a quantum many-body spin system. In particular, we study the Ising model in transverse field in the presence of a local field defect at one edge. This system possesses a rich phase diagram with different regions characterized by the presence of one or two Majorana zero modes. We show that their localized character *i*) enables a characterization of the Ising phase transition through a local-only measurement performed on the edge spin, and *ii*) strongly affects the propagation of quasiparticles emitted after the sudden removal of the defect, so that the dynamics of the local magnetization show clear deviations from a ballistic behavior in presence of the Majorana fermions.

PACS numbers:

The impressive progress made in the last two decades in the manipulation and detection of ultracold atomic gases, [1], has had a decisive rôle in pushing towards a better understanding of the dynamics of many body systems following a sudden quench, i.e. an abrupt change of some control parameter of the system. This has been the subject of many recent studies, focusing in particular on global quenches [2]. Examples of long studied systems and processes which have been realized with ultracold gases, range from the superfluid to Mott insulator transition [3] to the BCS to BEC crossover[4, 5]. A special emphasis in this respect deserve the studies of equilibration properties of interacting many body systems [6], including many interesting results such as the transition from diffusive to ballistic propagation dynamics of boson in a one dimensional lattice, [7]. The latter experiment is connected to one of the paradigm in the theory of global quenches in short ranged interacting many body systems, namely the existence of a maximum finite speed for the propagation of information within the system [8, 9]. On the other hand, a general understanding is still lacking in the case of local quenches, despite some interesting analysis for local bond quenches [10], for their connection to orthogonality catastrophe [11], for the study of local bound states in interacting systems [12], and for a recent work by Smacchia and Silva [13], discussing the propagation of magnetization after a local time dependent quench in the quantum Ising model.

In the same spirit, and motivated by the increasing experimental ability to perform single-site resolved addressing and detection [14], we study how a local quench affects both the static and dynamical properties of an Ising chain of $N$ spins in a transverse field $h$, which is homogenous everywhere but for a local defect at the boundary.

For a homogeneous field and in the thermodynamic limit, the Ising system would display a second order Quantum Phase Transition (QPT) at a critical value of the external field $h = h_c$, separating a paramagnetic phase with a non-degenerate ground state, from an interaction dominated, ordered phase, with a two-fold degenerate ground state. By means of a Jordan-Wigner transformation, the spin system can be mapped onto an homogeneous Kitaev chain [15], whose phase diagram has been studied in detail [16] and is known to display a topologically non-trivial phase, and a trivial one. The non-trivial phase is characterized by the presence of boundary Majorana fermions, which have been extensively studied both theoretically [17–19] and experimentally [20–22], also with the aim of exploiting them to implement topological quantum computation[23]. Global quench induced dynamics have been addressed for this system to study the transport of localized excitations between the two edges of the chain [24, 25], a necessary step to implement topological gates.

The magnetic field defect we consider gives a twofold effect: 1) the topological Majorana mode in the non-trivial phase gets distorted; 2) a localized eigenmode appears, which itself becomes a zero mode within a one-dimensional subregion of the otherwise trivial topological phase. As a consequence, the phase diagram in presence of the defect becomes much richer, due to the presence of either one or two of these localized modes. Finally, when the defect is quenched off, quasiparticles are "emitted" from a finite region around it and propagate throughout the system showing a clear signature of the presence of the Majorana mode.

## I. MODEL AND PHASE DIAGRAM

We consider the transverse field Ising model with open boundary conditions in the presence of a local dip in the magnetic field (a *defect*), described by the Hamiltonian:

$$H_\mu = -J\Big\{h\sum_{n=2}^{N}\hat{\sigma}_n^z - \sum_{n=1}^{N-1}\hat{\sigma}_n^x\hat{\sigma}_{n+1}^x + \mu h\,\hat{\sigma}_1^z\Big\}, \quad (1)$$

where $\mu$ is used to parameterize the field defect, and we scaled the magnetic field so that $h_c$=1. From now on, we take the exchange constant as our energy unit, $J = 1$. Despite the breaking of both translation invariance and reflection symmetry, $H_\mu$ can be diagonalized in terms of fermion operators $\eta_k$,

$\eta_k^\dagger$, (the diagonalization, based on [26–28], is discussed in the Appendix)

$$H_\mu = \sum_\kappa \Lambda_\kappa \eta_\kappa^\dagger \eta_\kappa + \chi_1 \Lambda_1 \eta_1^\dagger \eta_1 + \chi_2 \Lambda_2 \eta_2^\dagger \eta_2 \,, \qquad (2)$$

where $\kappa$ runs over a quasi-continuous band of delocalized modes, while two further *discrete* modes can appear depending on the value of the magnetic field $h$ and of the defect parameter $\mu$. Let $\mathcal{R}_n$ be the region in parameter space where mode $n = 1, 2$ exists; then, $\mathcal{R}_1$ is the ferromagnetic region $h \leq 1$, while $\mathcal{R}_2 = \{(h,\mu) : (\forall h \wedge |\mu| > \sqrt{1+1/h}) \vee (h > 1 \wedge |\mu| < \sqrt{1-1/h})\}$, see Fig. (1) and the Appendix. In Eq. (2), $\chi_1 = \Theta(1-h)$ and $\chi_2$ are the characteristic functions of these two regions, so that the corresponding fermion mode $n = 1$ ($n = 2$) is absent if $h, \mu$ are taken outside $\mathcal{R}_1$ ($\mathcal{R}_2$). These two modes, have frequency

$$\Lambda_1 = \frac{2\mu(1-h^2)h^N}{\sqrt{|1+(\mu^2-1)h^2|}} \,, \quad \Lambda_2 = 2\,|\mu| \sqrt{\frac{1+(\mu^2-1)h^2}{(\mu^2-1)}} \,. \qquad (3)$$

Mode 1 originates from fermion pairing, as found by Kitaev [15] for a homogeneous system. In our case, it is distorted by the presence of the defect (i.e. if $\mu \neq 1$), both in its energy and in its spatial structure. It becomes a zero mode in the thermodynamic limit, remaining spatially localized on the boundaries of the chain for any value of $\mu$. Mode 2 originates from the defect, it is discrete and localized too; its energy can lie either below or above the band (lower or upper of the yellow subregions in Fig. 1, respectively). If $\mu = 0$, $\Lambda_2$ becomes zero even at finite size; as a result, the real fermion operators $\eta_2^{(a)}$ and $\eta_2^{(b)}$ defined as $\eta_2 = \eta_2^{(a)} + i\eta_2^{(b)}$ decouple from the Hamiltonian, so that mode 2 becomes a Majorana zero mode, localized around the defect (see Table (IA) in the Appendix).

The presence of such localized structures affects all of the static properties of the system. In particular, we will focus on the local transverse magnetization that, in the Jordan-Wigner language, is related to fermion occupation. As shown in Fig. 2, the defect-localized mode maintains a non-vanishing magnetization on the first site for every finite value of $\mu$. In particular, $\langle S_1^z \rangle$ grows linearly with the external magnetic field with a slope proportional to $\mu$ far from criticality. For $\mu \to 0$, however, we obtain a singular behavior, $\lim_{\mu \to 0^\pm} \langle S_1^z \rangle = \mp \frac{\sqrt{h^2-1}}{2h} \Theta(h-1)$, whose step-like nature originates from a discontinuity in the spatial structure of mode 2 in the paramagnetic region, see also the Appendix. The fact that the magnetisation is zero (for vanishing $\mu$) in the ferromagnetic region can be qualitatively justified by observing that the spin-spin interaction locally dominates in this case, preventing the impurity spin to acquire a finite magnetisation in the $z$-direction. On the contrary, in the paramagnetic regime, the one-body Hamiltonian term dominates in Eq. 1, resulting in a building-up of $\langle S_1^z \rangle$ even for vanishingly small $\mu$.

Because of these features, the impurity spin and its magnetization behave as a local probe, able to detect the bulk properties of the spin chain: for $\mu = 0$, $\langle S_1^z \rangle$ is zero in the ordered phase, while it is different from zero in the disordered one. This is quite peculiar as, in general terms, for a second-order QPT as the one we are facing here, critical properties are exhibited in the bulk, and no *local* measurement of the transverse magnetization or of its susceptibility close to the boundary is able to pinpoint the QPT. On the other hand, we have just shown that the local magnetization on the edge impurity site is able to capture and signal the QPT.

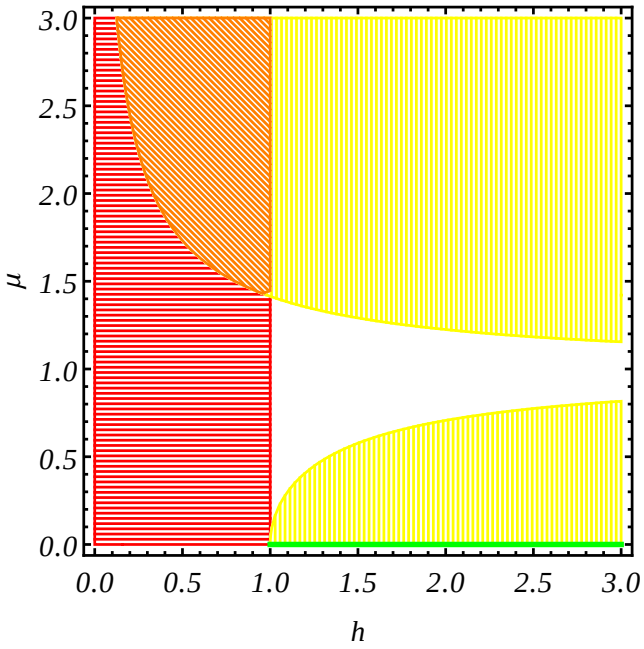


Figure 1: (Color online): Phase diagram showing the presence of the localized modes $\Lambda_n$ ($n$=1, 2) in the $h, \mu$ plane. The red region (horizontal lines), $\mathcal{R}_1$, features the presence of the mode with energy $\Lambda_1$. The yellow region (vertical lines) $\mathcal{R}_2$, instead, features the presence of mode 2, either below or above the band in the two subregions with $\mu$ smaller or larger than $\mu = 1$, respectively. Both of the localized modes are present in the orange region (oblique lines), corresponding to the intersection of $\mathcal{R}_1$ and $\mathcal{R}_2$. On the solid green line ($\mu = 0$ with $h \geq 1$) we have $\Lambda_2 = 0$ and mode 2 becomes a zero mode. Finally, only delocalized modes are present in the white region.

## II. PROPAGATION OF QUASI-PARTICLES

We now turn to the study of the dynamics following the sudden removal of the defect on the first site. The aim is to discuss how a local perturbation propagates in the system and, in particular, how the dynamics is affected by the Majorana zero mode. To this end, we assume the system to be initially prepared in the ground state $|GS\rangle_0$ of $\hat{H}_0$ (with $\mu = 0$). At $t = 0$ the defect is suddenly removed ($\mu = 1$ for $t \geq 0$), so that the system's subsequent evolution is generated by the homogeneous Ising Hamiltonian $\hat{H}_1$, whose ground state we denote $|GS\rangle_1$.

The spatial structure of the initial state $|GS\rangle_0$ differs from that of $|GS\rangle_1$ near the first site only. To characterize the local

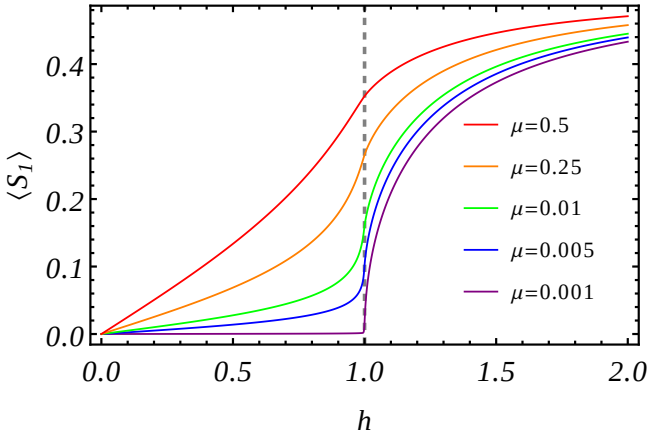


Figure 2: (Color online): Transverse magnetization of the defect spin as a function of the magnetic field for various defect's strength $\mu$ (with $\mu$=1 corresponding to a homogeneous system), for $N = 1000$.

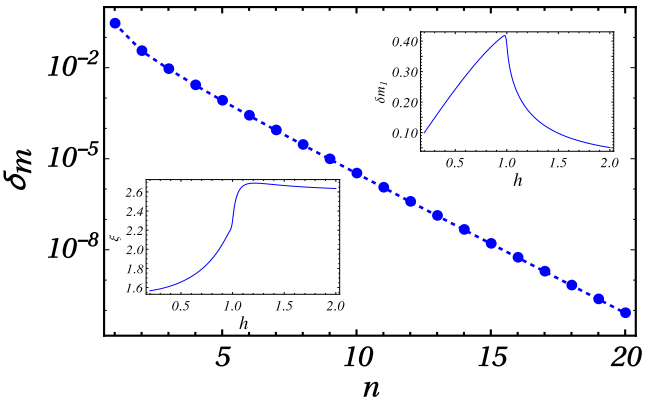


Figure 3: (Color online): Magnetization change $\delta m$ between the ground states of the final and initial Hamiltonians for $N = 200$ spins and $h = 0.6$. Insets: (top) magnetization change at the first site, $\delta m_1$, as a function of $h$; (bottom) localization length $\xi$.

differences between these two states we employ the magnetization contrast $\delta m_i = \langle \hat{S}_i^z \rangle_{GS_1} - \langle \hat{S}_i^z \rangle_{GS_0}$, which quantifies the defect-induced perturbation of the ground state with respect to the homogeneous field Hamiltonian $\hat{H}_1$ at a given $h$. We expect the two ground states to look very similar far from the defect site and to differ significantly only around it. Indeed, $\delta m_i$ decays exponentially with the distance from the defect, $\delta m_i = \delta m_1 \exp(-(i-1)/\xi)$, with a short localization length $\xi$, see Fig.3. Notice, in particular, that the perturbation is always localized within the first three sites regardless of the value of $h$. On the other hand, $\delta m_1$ increases with $h$ for $0 < h < 1$ while it goes to zero for $h > 1$ away from the critical point (indeed, in the paramagnetic phase, the magnetization tends to saturate with increasing $h$, both with and without the defect).

Once the defect is removed, the local magnetization peak travels through the chain, starting near site $i = 1$ at $t = 0$. In fact, we can think of the region of size $\xi$ around the first site as a source of quasi-particles that carry magnetization and correlations [9, 13].

Two different scenarios occur, depending on the value of the transverse field $h$. For $h > 1$, after the quench the system only supports delocalized fermion eigen-modes (white region in Fig.1). These will be shown to give rise to a purely ballistic propagation of the magnetization peak. In the ordered phase $0 < h < 1$, on the other hand, $H_1$ enjoys the localized mode with energy $\Lambda_1$, residing on the edge of the system, and substantially overlapping with the initial localized state $|GS\rangle_0$. A pinning of the excitation near the first site occurs in this case, due to the interplay of the otherwise ballistic propagation with the localized nature of the Majorana mode, and giving rise to temporal oscillations of the local magnetization.

In order to characterize the propagation of the magnetic perturbation along the chain, we consider the mean square magnetization center and its velocity, defined as

$$R^2(t) = \sum_{i=1}^{N} \delta m_i(t)(i-1)^2 \tag{4}$$

$$v(t) = \frac{d}{dt}\sqrt{|R^2(t) - R^2(0)|}. \tag{5}$$

where $\delta m_i(t) = \langle \hat{S}_i^z \rangle_{GS_1} - \langle \hat{S}_i^z(t) \rangle_{GS_0}$ is the time-dependent version of the magnetization contrast introduced above. Analogous variables have been adopted and experimentally measured in Ref. [7].

Using the diagonal form of $H_1$, one can show that

$$R^2(t) = \sum_{k_1,k_2} A_{k_1\,k_2} \cos\left((\Lambda_{k_1} - \Lambda_{k_2})t\right) + \sum_{k_1,k_2} B_{k_1\,k_2} \cos\left((\Lambda_{k_1} + \Lambda_{k_2})t\right)$$

where the summations are performed over the eigenmodes of the final Hamiltonian $H_1$, including both the delocalized fermion modes $\kappa$ forming a band in the thermodynamic limit, and, if $h < 1$, the (Majorana) edge mode $n = 1$. The explicit form of the matrices $A$ and $B$ are given in the Appendix; what is important here is that they give two different types of contribution to the propagating magnetization center: a rotating term, $(A)$, and a counter-rotating one, $(B)$. The former fully determines the asymptotic behavior of $R(t)$, as the $B$-contribution becomes negligible at long times due to their fast oscillations. This is clearly seen in Fig.4, where we show $\delta R(t) = \sqrt{R^2(t) - R^2(0)}$ for different values of the magnetic field $h$. In the plots, the solid blue curves giving $\delta R(t)$ are compared to the behaviors obtained by artificially keeping the rotating terms only in the rhs of Eq.(4). This is done to better emphasize that $B$-terms only contribute to the transient oscillations, after which the propagation is ballistic and completely accounted for by the rotating terms. Furthermore,

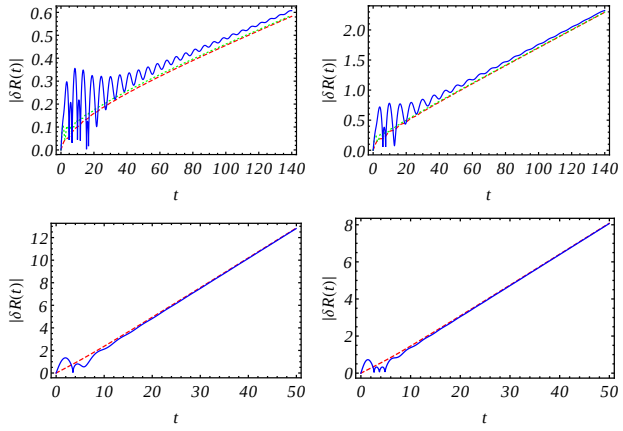


Figure 4: (Color online): Detachment of the magnetization center from its initial position, $\delta R(t) = \sqrt{R^2(t) - R^2(0)}$, for (top left to bottom right) $h = 0.4, 0.6, 1.2, 1.6$, with $N = 100$. Solid blue lines are drawn by using the full expression for $R(t)$, whereas dashed red lines contain the rotating $(A)$ contributions only. The dashed green lines are obtained from the blue ones by artificially excluding the contribution from the Majorana zero mode, in order to better highlight its role.

by analyzing the matrix $A$ as displayed in Fig. (5), we see that the main contribution comes from the entries close to the diagonal, so that the long-time speed is

$$\bar{v} \approx \sqrt{\sum_{\kappa} \frac{A_{\kappa\,\kappa+1}}{2} \left(\Lambda_{\kappa} - \Lambda_{\kappa+1}\right)^2}\,.$$

This gives a very good approximation for the average propagation velocity in the disordered region, while it fails near the critical point, where $\delta R(t)$ and $v(t)$ keep oscillating even at long times, see Fig. (6), and in the ordered region, because of the presence of the Majorana mode, coming into play via the counter rotating terms.

In fact, the $B$ contributions are worth analyzing in some detail. They are basically irrelevant for $h > 1$, while their presence induces strong transient oscillations in the ferromagnetic phase, whose amplitude increases as $h \to 1^-$. This is essentially due to the presence of the Majorana mode. Indeed, Fig. (5) clearly shows that in the ordered phase ($h < 1$), the only contribution of the $B$-type comes from the coupling between the $n = 1$ mode and the delocalized ones. Furthermore, in Fig. (4), for $h < 1$ (top panels) we can see that, if all of the terms involving the Majorana zero mode were excluded from the sum in Eq. (4), then the oscillations would disappear (as seen by comparing the dotted green curves with the solid blue ones). Therefore, it is the presence of the Majorana mode in the final Hamiltonian that gives rise to the large and persistent fluctuations in $\delta R(t)$, which can be understood as a result of the localized mode tieing the magnetization peak at short times.

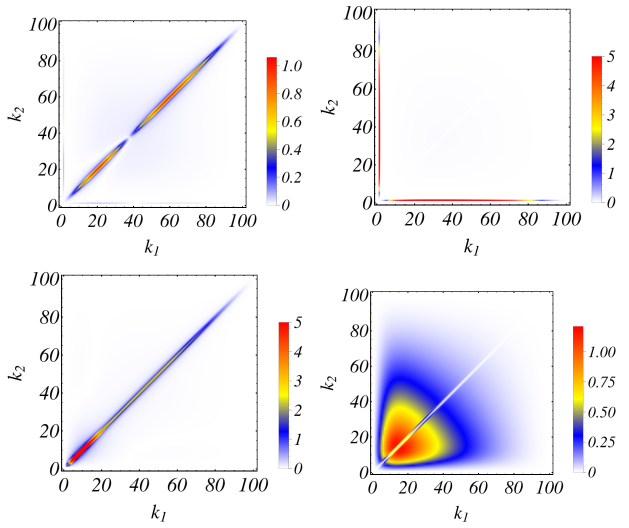


Figure 5: (Color online): Elements of the matrices $A$ (left panels) and $B$ (right ones) for $h = 0.4$ (top) and $h = 1.4$ (bottom). The plots are made for $N = 100$.

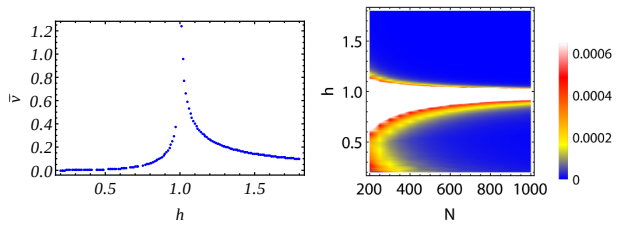


Figure 6: (Color online): Left: Average asymptotic speed $\bar{v}$, taken in the long time limit (but before the occurrence of finite size revivals) as a mean over residual long time oscillations, for $N = 800$. Right: Scaling with the system size $N$ and with the external field $h$ of the amplitude of the long time oscillations displayed by the propagation speed $v(t)$ around the average $\bar{v}$. In the white region the limiting speed is not well defined because of the persistence of its oscillations.

## III. CONCLUSIONS

To summarize, we studied the effect of a local magnetic field defect on both the static and dynamic properties of the Ising model in transverse field $h$. The excitation spectrum of this system is made of a continuous band of delocalized states and, depending on the interplay between the external field $h$ and the defect parameter $\mu$, of up to two localized modes. We have shown that for $0 < h < 1$ the defect modifies the wave function of the (Kitaev) fermion paring induced Majorana mode, and that it can give rise to a new localized zero mode in the disordered region; furthermore, we demonstrated that, in the limit of a vanishing magnetic field on the edge, the Ising critical point can be detected by means of local measurement on the impurity. We have also studied the propagation of local magnetic excitations occurring after the defect is quenched off and showed that the propagation is ballistic but for some oscillations induced by the the Majorana mode for

$0 < h < 1$, whose effect persist at long times near the critical point.

*Acknowledgments* - We are grateful to T. Alecce and L. Dell'Anna for helpful discussions, and acknowledge financial support by the EU Collaborative project QuProCS (Grant Agreement 641277). T.J.G.A. acknowledges funding under the EU Collaborative Project TherMiQ (Grant No. 618074)

## Appendix A

### 1. Diagonalization of the Ising model with an edge defect

The Ising model with a magnetic field inhomogeneity at one edge is given by

$$\hat{H} = -\mu h\, \hat{\sigma}_1^z - h \sum_{n=2}^{N} \hat{\sigma}_n^z + \sum_{n=1}^{N-1} \hat{\sigma}_n^x \hat{\sigma}_{n+1}^x \,, \tag{A1}$$

where $\hat{\sigma}_n^\alpha$ ($\alpha$=$x, y, z$) are the usual Pauli spin operator on site $n$, and $h > 0$. Diagonalization of Eq. A1 is achieved first by introducing the non-local Jordan-Wigner (J-W) transformation [26]

$$\hat{\sigma}_n^z = 2\hat{c}_n^\dagger \hat{c}_n - 1, \tag{A2}$$

$$\hat{\sigma}_n^- = e^{i\pi \sum_{j=1}^{n-1} \hat{c}_j^\dagger \hat{c}_j} \hat{c}_n, \tag{A3}$$

$$\hat{\sigma}_n^+ = e^{-i\pi \sum_{j=1}^{n-1} \hat{c}_j^\dagger \hat{c}_j} \hat{c}_n^\dagger, \tag{A4}$$

where $\hat{\sigma}_j^\pm$=$(\hat{\sigma}_j^x \pm i\hat{\sigma}_j^y)/2$ are the raising and lowering spin operator. This transformation fermionizes Eq. A1 into

$$\hat{H} = \sum_{i\,j} \left( \hat{c}_i^\dagger A_{i\,j} \hat{c}_j + \frac{1}{2} \left( \hat{c}_i^\dagger B_{i\,j} \hat{c}_j^\dagger + h.c. \right) \right) \tag{A5}$$

where $A$ and $B$ are tridiagonal symmetric and anti-symmetric matrices respectively, whose elements are given by $A_{i\,j}$=$2h\left((\mu+1)\,\delta_{i1}-1\right)\delta_{ij} - (\delta_{i\,j+1}+\delta_{i+1\,j})$ and $B_{i\,j} = (\delta_{i\,j+1}-\delta_{i+1\,j})$. Since the Hamiltonian in Eq. A5 is bilinear in the creation and annihilation operators it can be diagonalized by means of a Bogoliubov transformation:

$$\hat{c}_i = \sum_k u_{ik} \hat{\eta}_k + v_{ik} \hat{\eta}_k^\dagger \tag{A6}$$

with the conditions $\sum_k u_{ik}u_{jk} + v_{ik}v_{jk} = \delta_{ij}$ and $\sum_k u_{ik}v_{jk} + v_{ik}u_{jk} = 0$ to ensure that the transformation is canonical and preserves the anti-commutation relations. From the equations of motion for the operators $\hat{c}_i$ (or equivalently for $\hat{c}_i^\dagger$), the Bogoliubov transformation in Eq.A6 and imposing the time dependence $\eta_k(t) = \eta_k e^{-\imath\Lambda_k t}$ for the normal modes we obtain the following equations for the element of the transformation matrices $u$ and $v$:

$$\sum_j A_{ij}u_{jk} + B_{ij}v_{jk} = \Lambda_k u_{ik} \tag{A7}$$

$$\sum_j B_{ij}u_{jk} + A_{ij}v_{jk} = -\Lambda_k v_{ik}. \tag{A8}$$

The Hamiltonian rewritten in terms of the normal modes reads $\hat{H} = \sum_k \Lambda_k \hat{\eta}_k^\dagger \hat{\eta}_k - Nh + (\mu+1)h - \frac{1}{2}\sum_k \Lambda_k$.

In view of the discussion about the Majorana modes we introduce the new matrices $\phi = u^T + v^T$ and $\psi = u^T - v^T$ whose column vectors satisfy the equations:

$$\begin{cases} (A+B)\,\vec{\phi}_k = \Lambda_k \vec{\psi}_k \\ (A-B)\,\vec{\psi}_k = \Lambda_k \vec{\phi}_k \end{cases} . \tag{A9}$$

*In the absence of impurity* the above equations can be decoupled, yielding respectively:

$$M_1 \vec{\psi}_k = \Lambda_k^2 \vec{\psi}_k \quad \text{or} \quad M_1^{'} \vec{\phi}_k = \Lambda_k^2 \vec{\phi}_k \,, \tag{A10}$$

where $M_1$=$(A+B)(A-B)$ and $M_1^{'}$=$(A-B)(A+B)$ turns out to be the mirror-inverted matrix $M_1^{'}$=$R^\dagger M_1 R$, with $R$ denoting the reflection operator $R_{i\,j}$=$\delta_{i\,2N+1-j}$. Because of the open boundary conditions, $M_1$ ($M_1^{'}$) are symmetric tridiagonal matrices uniform along the diagonals but for the first (last) element on the main one. The position of this non-uniformity makes it possible to determine analytical solutions for the spectrum of $M$ [27, 28].

The presence of the impurity $\mu$ breaks the mirror-inversion symmetry and therefore the diagonalization procedures for $M_\mu$ or $M_\mu'$, although numerically possible even for large $N$, are different. In fact, $(A-B)(A+B)$ turns out to be a real, tridiagonal matrix with the upper corner (*i.e.*, the matrix elements $\{(1,1),(1,2),(2,1)\}$) depending on $\mu$, and this, to the best of our knowledge, does not admit an analytical solution for arbitrary values of $\mu$. The matrix $M_\mu$=$(A+B)(A-B)$, instead, has only the first element on the main diagonal depending on $\mu$ (beside a $\mu$-independent non-uniformity on the last element of the same diagonal). As a consequence, the latter is prone to analytical diagonalization for arbitrary values of the impurity strength by means of the technique outlined in Ref. [27].

The matrix $M_\mu$=$(A+B)(A-B)$ is positive, tridiagonal, and symmetric, and reads

$$M = \begin{pmatrix} b-\alpha & a & 0 & \cdots & 0 \\ a & b & a & \cdots & 0 \\ 0 & a & b & \cdots & \cdots \\ \cdots & \cdots & \cdots & \cdots & \cdots \\ 0 & \cdots & a & b & a \\ 0 & \cdots & 0 & a & b-\beta \end{pmatrix} , \tag{A11}$$

with $b = 4 + 4h^2$, $a = -4h$, $\alpha = 4h^2(1-\mu^2)$, $\beta = 4$. Lengthy, but straightforward, calculations lead to the follow-

ing equation

$$a(\alpha+\beta)\sin(N\theta_k)+a^2\sin\left[(N+1)\theta_k\right]+\alpha\beta\sin\left[(N-1)\theta_k\right]=0 \tag{A12}$$

where $\theta_k\in\mathbb{C}$ is related to the eigenvalues $\Lambda_k$ of Eqs. A10 by $\cos\theta_k=\frac{\Lambda_k^2-b}{2a}$, with the index $k$ labelling the energy levels. Finally we solve Eq. A12 in the limit $N\gg1$. Having obtained the allowed $\theta_k$, the problem is solved and the matrices $\psi$ and $\phi$ are obtained via Eqs. A10.

Depending on the values of the Hamiltonian parameters $\{h,\mu\}$, there can be up to two complex $\theta_k$, which give rise to the out-of-band energy levels reported in the main text. The phase diagram in the $\{h,\mu\}$-plane is made up of the following regions: $\mathcal{R}_1=\{(h,\mu)\,:\,0<h<1\}$ and $\mathcal{R}_2=\{(h,\mu)\,:\,(\forall h\wedge|\mu|>\sqrt{1+1/h})\vee(h>1\wedge|\mu|<\sqrt{1-1/h})\}$ A graphical representation of these regions is given in the main text. Results for the eigenvalues, and for the coefficients $\psi$ and $\phi$ are reported in Table A 1, for the various regions.

Table I: Expressions for the eigenvalues and the $\{\psi,\phi\}$ matrix elements in the $(h,\mu)$-plane.

| $(h,\mu)$ | $\Lambda$ | $\psi$ | $\phi$ |
|---|---|---|---|
| $\forall(h,\mu)$ | $\Lambda_\kappa=2\sqrt{1+h^2-2h\cos\theta_\kappa}$ | $\psi_n(\theta_\kappa)=\sqrt{\frac{2}{N}}\frac{\sin(n\theta_\kappa)+(\mu^2-1)h\sin((n-1)\theta_\kappa)}{\sqrt{1+(\mu^2-1)^2h^2+2h(\mu^2-1)\cos\theta_\kappa}}$ | $\phi_n(\theta_\kappa)=\frac{2h}{\Lambda_\kappa}\psi_n(\theta_\kappa)-\frac{2(\mu+1)h\delta_{n1}}{\Lambda_\kappa}\psi_1(\theta_\kappa)-\frac{2(1-\delta_{n1})}{\Lambda_\kappa}\psi_{n-1}(\theta_\kappa)$ |
| $\mathcal{R}_1$ | $\Lambda_1=\frac{2\lvert\mu\rvert(1-h^2)h^N}{\sqrt{\lvert1+(\mu^2-1)h^2\rvert}}$ | $\psi_n^{(1)}=\sqrt{1-h^2}\left(h^{N-n}-\frac{\mu^2h^{N+n}}{1+(\mu^2-1)h^2}\right)$ | $\phi_n^{(1)}=\frac{\sqrt{1-h^2}\sqrt{\lvert1+(\mu^2-1)h^2\rvert}}{\lvert\mu\rvert h(1+(\mu^2-1)h^2)}\left(1-(\mu+1)\left(\delta_{n1}+(1-\delta_{n1})\right)(1-\mu)\right))h^n$ |
| $\mathcal{R}_2$ | $\Lambda_2=2\lvert\mu\rvert\sqrt{\frac{1+(\mu^2-1)h^2}{(\mu^2-1)}}$ | $\psi_n^{(2)}=\frac{(-1)^nh^{-n}\sqrt{(\mu^2-1)^2h^2-1}}{(\mu^2-1)^n}$ | $\phi_n^{(2)}=\frac{2h}{\Lambda^{(2)}}\psi_n^{(2)}-\frac{2(\mu+1)h\delta_{n1}}{\Lambda^{(2)}}\psi_1^{(2)}-2\frac{1-\delta_{n1}}{\Lambda^{(2)}}\psi_{n-1}^{(2)}$ |

The first line of Table A 1, where

$$\theta_k=\frac{k\pi}{N}+\frac{1}{N}\arctan\left(\frac{h\mu^2\sin\left(\frac{k\pi}{N}\right)}{((\mu^2-1)h-1)+h(2-\mu^2)\cos\left(\frac{k\pi}{N}\right)}\right), \tag{A13}$$

with $k\in\mathbb{Z}$, refers to spatially delocalized energy modes having energy in the interval $E_b=[2\lvert1-h\rvert,2\lvert1+h\rvert]$. For finite systems, there are $N,N-1$, or $N-2$ modes depending on location in the $(h,\mu)$-plane. For infinite systems, on the other hand, they build up an energy band with a gap equal to $2\lvert1-h\rvert$ closing at the QPT point $h_c=1$. The second line shows the zero-energy mode (in the $N\to\infty$ limit) and the corresponding Majorana localized eigenstate which is extensively discussed in the main text. Finally, the last line reports an energy level appearing above (or below) the band for $(h,\mu)\in\mathcal{R}_2$. The corresponding eigenstate turns out to be localized only around the impurity and has a finite energy but on the line $\mu=0$ where it vanishes $\forall h$. The occurrence of $\Lambda^{(2)}=0$ implies a discontinuity for $\phi_1^{(2)}$ and a non-differentiable point for $\phi_n^{(2)}$ with $n>1$. Indeed, $\phi_1^{(2)}=-\frac{2\mu h}{\Lambda^{(2)}}\sqrt{1-((\mu^2-1)h)^{-2}}$ and $\phi_n^{(2)}=\frac{2h\mu^2}{\Lambda^{(2)}}\left((\mu^2-1)h\right)^{-n}\sqrt{\left((\mu^2-1)h\right)^2-1}$.

By introducing two (real) Majorana operators on each site: $\hat{a}_n=\hat{c}_n+\hat{c}_n^\dagger$ and $\hat{b}_n=i(\hat{c}_n^\dagger-\hat{c}_n)$ together with the Bogoliubov transformations in Eq.A6 we have

$$\hat{a}_n=\sum_\kappa\phi_n(\theta_\kappa)\hat{\alpha}_\kappa+\sum_i\phi_n^{(i)}\hat{\alpha}_i \tag{A14}$$

$$\hat{b}_n=\sum_\kappa\psi_n(\theta_\kappa)\hat{\beta}_\kappa+\sum_i\psi_n^{(i)}\hat{\beta}_i \tag{A15}$$

where we defined the Majorana modes $\hat{\alpha}_k=\hat{\eta}_k^\dagger+\hat{\eta}_k$ and $\hat{\beta}_k=i(\hat{\eta}_k^\dagger-\hat{\eta}_k)$ and the functions $\phi$ and $\psi$ are given in Table (A 1).

The Hamiltonian thus reads:

$$\hat{H}_\mu=i\mu h\,\hat{a}_1\hat{b}_1+ih\sum_{n=2}^{N}\hat{a}_n\hat{b}_n-i\sum_{n=1}^{N-1}\hat{a}_{n+1}\hat{b}_n. \tag{A16}$$

In this form it is easy to see that for $\mu=0$ the Majorana operators $\hat{a}_1$ and $\hat{b}_1$ both commute with the Hamiltonian.

### 2. Transverse magnetization

The magnetization is given by $\left\langle\hat{S}_n^z\right\rangle=\frac{\langle\hat{\sigma}_n^z\rangle}{2}=\frac{1}{2}-\left\langle\hat{c}_n^\dagger\hat{c}_n\right\rangle$. By inverting Eq. A6 and exploiting the property $\eta_k\lvert GS\rangle=0$, $\forall k$, we are left with $\left\langle\hat{S}_n^z\right\rangle=\frac{1}{2}-\sum_k v_{kn}^2$. In the thermodynamic limit $N\to\infty$, we obtain the exact result

$$\left\langle\hat{S}_n^z\right\rangle=\tfrac{1}{2}-\Big[\int_0^\pi d\theta\,v_n^2(\theta)+\Theta(h-1)\,\Theta(x^+)\,\Theta(y^+)\left(v_n^{(2)}\right)^2 \\ +\Theta(1-h)\left(\left(\Theta(y^-)+\Theta(x^-)\right)\left(v_n^{(2)}\right)^2+\left(v_n^{(1)}\right)^2\right)\Big], \tag{A17}$$

where $v_n^{(i)}$ is the Bogoliubov coefficient relative to the discrete mode $i=1,2$, while $x^\pm=\mu\pm\sqrt{h(h\mp1)}$, $y^\pm=\pm\sqrt{h(h\mp1)}-\mu$, and $\Theta(x)$ is the Heaviside step function.

Let us focus on the case $\mu\to0$. Eq. A17 can be evaluated analytically as the contribution of the continuous modes in the

integrand, given by

$$v_n^2(\theta) = \frac{1}{2\pi f^2}\Big[-h\,\widetilde{\sin}\left((n-2)\,\theta\right) + \left(1+h^2-h\,f\right)\widetilde{\sin}\left((n-1)\,\theta\right) + (f-h)\,\widetilde{\sin}\left(n\theta\right)\Big]\,, \tag{A18}$$

where $f\equiv f(h,\theta)=\sqrt{1+h^2-2h\cos\theta}$ and the modified trigonometric function reads $\widetilde{\sin}(x)=\Theta(x)\sin(x)$, results in rational functions of $h$ times complete elliptic integrals of the first and second kind for $n\geq 2$. For the sake of brevity, we do not report the result for arbitrary $n$ of Eq. A17, but, rather, focus on the case $n=1$, which reads

$$\begin{aligned}\lim_{\mu\to 0^{\pm}}\left\langle \hat{S}_1^z\right\rangle &= \frac{1}{2}-\frac{1}{8h^2}\left(1+Sg\left(h-1\right)+h^2\left(1+Sg\left(1-h\right)\right)\right)\\ &-\Theta\left(h-1\right)\frac{2h\left(h\mp\sqrt{h^2-1}\right)-1}{4h^2}-\frac{\Theta\left(1-h\right)}{4}\\ &= \mp\,\frac{\sqrt{h^2-1}}{2h}\Theta(h-1)\,,\end{aligned} \tag{A19}$$

where $Sg(x)$ is the sign function.

### 3. Coupling matrices

In the first section of this Appendix, we have shown how to diagonalize an Hamiltonian having the form in Eq. A5. When performing a sudden quench both the initial and the final Hamiltonian have this form and can thus be diagonalized following the above procedure. To this end, we need two Bogoliubov transformations as in Eq.A6:

$$\hat{c}_i = \sum_i u_{ik}\hat{\eta}_k + v_{ik}\hat{\eta}_k^{\dagger} \tag{A20}$$

$$\hat{c}_i = \sum_i w_{ik}\hat{\xi}_k + z_{ik}\hat{\xi}_k^{\dagger} \tag{A21}$$

where again we require $\sum_k u_{ik}u_{jk} + v_{ik}v_{jk} = \delta_{ij}$ and $\sum_k w_{ik}w_{jk}+z_{ik}z_{jk}=\delta_{ij}$. Using these relations and the transformations above we can write:

$$\begin{pmatrix}\hat{\xi}_k\\ \hat{\xi}_k^{\dagger}\end{pmatrix} = \sum_k \begin{pmatrix}U_{kq} & V_{kq}\\ V_{kq} & U_{kq}\end{pmatrix}\begin{pmatrix}\hat{\eta}_q\\ \hat{\eta}_q^{\dagger}\end{pmatrix} \tag{A22}$$

where

$$U_{kq} = \sum_i w_{ik}u_{iq} + z_{ik}v_{iq} \tag{A23}$$

$$V_{kq} = \sum_i z_{ik}u_{iq} + w_{ik}v_{iq}. \tag{A24}$$

Thanks to the above expression it is now easy to recover the expression in the main text for the mean local number of fermions at site $i$:

$$\langle \hat{c}_i^{\dagger}(t)\hat{c}_i(t)\rangle = \sum_{k_1,k_2} A^{(i)}_{k_1k_2}\cos\left(\left(\Lambda_{k_1}-\Lambda_{k_2}\right)t\right) \tag{A25}$$

$$+ \sum_{k_1,k_2} B^{(i)}_{k_1k_2}\cos\left(\left(\Lambda_{k_1}+\Lambda_{k_2}\right)t\right) \tag{A26}$$

where

$$A^{(i)}_{k_1k_2} = \left(w_{ik_1}w_{ik_2}-z_{ik_1}z_{ik_2}\right)\sum_l V_{k_1l}V_{k_2l} \tag{A27}$$

$$B^{(i)}_{k_1k_2} = 2w_{ik_1}z_{ik_2}\sum_l U_{k_1l}V_{k_2l}. \tag{A28}$$

The matrices $A$ and $B$ in the definition of $R^2(t)$ in the main text are given by

$$A_{k_1k_2} = \sum_i A^{(i)}_{k_1k_2}(i-1)^2 \tag{A29}$$

$$B_{k_1k_2} = \sum_i B^{(i)}_{k_1k_2}(i-1)^2. \tag{A30}$$


[1] I. Bloch, J. Dalibard, W. Zwerger, Rev. Mod. Phys. **80**, 885 (2008).

[2] A. Polkovnikov, K. Sengupta, A. Silva, and M. Vengalattore, *Nonequilibrium dynamics of closed interacting quantum systems*, Rev. Mod. Phys. **83**, 863 (2011); J. Eisert, M. Friesdorf, C. Gogolin, *Quantum many-body systems out of equilibrium*, Nature Phys. **11**, 124 (2015).

[3] M. A. Cazalilla, R. Citro, T. Giamarchi, E. Orignac, and M. Rigol, *One dimensional bosons: From condensed matter systems to ultracold gases*, Rev. Mod. Phys. 83, 1405 (2011).

[4] C. A. Regal, M. Greiner, S. Giorgini, M. Holland, and D. S. Jin, *Momentum distribution of a Fermi gas of atoms in the BCS-BEC crossover*, Phys. Rev. Lett. **95**, 250404 (2005)

[5] W. Zwerger (ed), *The BCSBEC Crossover and the Unitary Fermi Gas*, Lecture Notes in Physics Vol. 836 (Springer, 2012).

[6] C. Gogolin, J. Eisert, *Equilibration, thermalisation, and the emergence of statistical mechanics in closed quantum systems*, Rep. Prog. Phys. 79, 056001 (2016).

[7] J. P. Ronzheimer, *et al*, *Expansion Dynamics of Interacting Bosons in Homogeneous Lattices in One and Two Dimensions*, Phys. Rev. Lett. **110**, 205301 (2013)

[8] E. Lieb, D. Robinson, *The finite group velocity of quantum spin systems*, Commun. Math. Phys. **28**, 251 (1972); M. Cheneau, P. Barmettler, D. Poletti, M. Endres, P. Schauss, T. Fukuhara, C. Gross, I. Bloch, C. Kollath, S. Kuhr, *Lightcone-like spreading of correlations in a quantum many-body system*, Nature **481**,

484 (2012); L. Bonnes, F. H. L. Essler, A. M. Läuchli, *"Light-Cone" Dynamics After Quantum Quenches in Spin Chains*, Phys. Rev. Lett. 113 187203 (2014).

[9] P. Calabrese, and J. Cardy, *Time Dependence of Correlation Functions Following a Quantum Quench*, Phys. Rev. Lett. **96**, 136801 (2006).

[10] U. Divakaran, F. Iglói, H. Rieger, *Non-equilibrium quantum dynamics after local quenches*, J. Stat. Mech. P10027 (2011); F. Iglói, G Roósz, L. Turban, *Evolution of the magnetization after a local quench in the critical transverse-field Ising chain*, J. Stat. Mech. P03023 (2014); T. J. G. Apollaro, F. Plastina, L. Banchi, A. Cuccoli, R. Vaia, P. Verrucchi, M. Paternostro, *Effective cutting of a quantum spin chain by bond impurities*, Phys. Rev. A **88**, 052336 (2013); T. J. G. Apollaro, A Cuccoli, A. Fubini, F. Plastina, and P. Verrucchi, *Staggered magnetization and entanglement enhancement by magnetic impurities in a $S = \frac{1}{2}$ spin chain*, Phys. Rev. A **77**, 062314 (2008).

[11] A. Silva, *Statistics of the Work Done on a Quantum Critical System by Quenching a Control Parameter*, Phys. Rev. Lett. **101**, 120603 (2008); A. Sindona, J. Goold, N. Lo Gullo, S. Lorenzo, F. Plastina, *Orthogonality catastrophe and decoherence in a trapped-Fermion environment*, Phys. Rev. Lett. **111**, 165303 (2013); A. Sindona, N. Lo Gullo, J. Goold, F. Plastina, *Statistics of the work distribution for a quenched Fermi gas*, New J. Phys. **16**, 045013 (2014); M. Schirò, A. Mitra, *Transient Orthogonality Catastrophe in a Time-Dependent Nonequilibrium Environment*, Phys. Rev. Lett. **112**, 246401 (2014).

[12] M. Ganahl, E. Rabel, F. H. L. Essler, H. G. Evertz *Observation of Complex Bound States in the Spin-1/2 Heisenberg XXZ Chain Using Local Quantum Quenches*, Phys. Rev. Lett. **108**, 077206 (2012); E. J. Torres-Herrera, L. F. Santos, *Local quenches with global effects in interacting quantum systems*, Phys. Rev. E **89**, 062110 (2014).

[13] P. Smacchia, and A. Silva, *Universal energy distribution of quasiparticles emitted in a Local time-dependent quench*, Phys. Rev. Lett. **109**, 037202 (2012).

[14] S. Hild, T. Fukuhara, P. Schauß, J. Zeiher, M. Knap, E. Demler, I. Bloch, C. Gross, *Far-from-Equilibrium Spin Transport in Heisenberg Quantum Magnets*, Phys. Rev. Lett. **113**, 147205 (2014).

[15] A. Kitaev, *Unpaired Majorana fermions in quantum wires*, Physics-Uspekhi **44**, 131 (2001).

[16] W. DeGottardi, M. Thakurathi, S. Vishveshwara, and D. Sen, *Majorana Fermions in superconducting wires: effects of long-range hopping, broken time-reversal symmetry and potential landscapes*, Phys. Rev. B **88**, 165111 (2013).

[17] D. E. Liu, and H. U. Baranger *Detecting a Majorana-fermion zero mode using a quantum dot*, Phys. Rev. B **84**, 201308(R) (2011).

[18] L. Fu, and C. L. Kane, *Probing Neutral Majorana Fermion Edge Modes with Charge Transport*, Phys. Rev. Lett. **102**, 216403 (2008).

[19] L. Jiang, *et al*, *Majorana Fermions in Equilibrium and in Driven Cold-Atom Quantum Wires*, Phys. Rev. Lett. **106**, 220402 (2011).

[20] A.R. Akhmerov, J. Nilsson, and C.W.J. Beenakker, *Electrically Detected Interferometry of Majorana Fermions in a Topological Insulator*, Phys. Rev. Lett. **102**, 216404 (2008).

[21] A. Das, *et al*, *Zero-bias peaks and splitting in an Al-InAs nanowire topological superconductor as a signature of Majorana fermions*, Nat. Phys. **8**, 887 (2012).

[22] V. Mourik, *et al*, *Signatures of Majorana Fermions in Hybrid Superconductor-Semiconductor Nanowire Devices*, Science **336**, 1003 (2012)

[23] S. Das Sarma, M. Freedman, C. Nayak, *Majorana zero modes and topological quantum computation*, npj Quantum Information **1**, 15001 (2015).

[24] W. DeGottardi, D. Sen, and S. Vishveshwara, *Topological phases, Majorana modes and quench dynamics in a spin ladder system*, New J. Phys. **13**, 065028 (2011).

[25] R. Vasseur, J.P. Dahlhaus, and J.E. Moore, *Universal Nonequilibrium Signatures of Majorana Zero Modes in Quench Dynamics*, Phys. Rev. X **4**, 041007 (2014).

[26] E. Lieb, T. Schultz, and D. Mattis, *Two soluble models of an antiferromagnetic chain*, Ann. Phys. (N. Y.) **16**, 406 (1961); P. Pfeuty, *The One-Dimensional Ising Model with a Transverse Field*, Ann. Phys. (N. Y.) **57**, 79 (1970); E. Barouch, B. McCoy, M. Dresden, *Statistical Mechanics of the XY Model. I*, Phys. Rev. A **2**, 1075 (1970); Barouch, B. M. McCoy, *Statistical Mechanics of the XY Model. II. Spin-Correlation Functions*, Phys. Rev. A **3**, 786 (1971).

[27] W.-C. Yueh, *Eigenvalues of Several Tridiagonal Matrices*, Appl. Math. E-Notes **5**, 6674 (2005).

[28] L. Banchi, and R. Vaia, *Spectral problem for quasi-uniform nearest-neighbor chains*, J. Math. Phys. **54**, 043501 (2013).